Progress In Electromagnetics Research, Vol. 143, 605–621, 2013

A STUDY OF RADAR FEATURES OF WIND TURBINES IN THE HF BAND

Aale Naqvi* **and Hao Ling**

Department of Electrical and Computer Engineering, The University of Texas at Austin, Austin, TX 78712-1084, USA

Abstract—Radar features of wind turbines are simulated and studied in the HF band. The features are presented in the range-Doppler plane for single as well as arrays of turbines. Doppler aliasing due to the limited pulse repetition frequency of HF radars is examined. Shadowing characteristics of arrays of turbines are simulated and analyzed. Electromagnetic modeling details including effects of thin-wire modeling, non-conducting turbine components, and the presence of a conducting ground surface are discussed.

1. INTRODUCTION

The growing number of wind farms worldwide has caused concerns due to their adverse effects on radar systems used for air defense, air traffic control, and weather. This has led to many studies documenting the interference due to wind farms on radar detection and tracking capabilities [1–11]. The electromagnetic scattering features of wind turbines in the microwave frequency range have also been studied and reported in detail [12–17]. Recently, concerns have been raised on the potential of offshore wind farms interfering with the existing high frequency (HF) radar networks built for ocean monitoring [18, 19]. In addition, the use of HF radars for monitoring the construction of offshore wind farms is being explored [19]. These interests necessitate a more in-depth understanding of how offshore wind farms interact with radar waves in the HF frequency range. For ocean current applications, HF radars operate in the frequency range of 3–50 MHz. Since the wavelengths in this frequency range (tens of meters) are comparable to the turbine size, the resulting scattering phenomenology may be quite different from earlier documented features in the microwave regime.

Received 31 October 2013, Accepted 24 November 2013, Scheduled 6 December 2013

* Corresponding author: Aale Naqvi (aalenaqvi@yahoo.com).

In [18], Wyatt et al. presented measured data on a Wellen Radar (WERA) system at 13 MHz of the Rhyl-Flats wind farm in UK's Liverpool Bay. Data from before and after the operation of the farm clearly showed the effect of the wind farm in raising the background clutter relative to the ocean Doppler return. This may affect the HF radar's ocean current and wave mapping capabilities, especially for some coastal ocean environments where the signal-to-noise-ratio of radar backscatter is low [20]. In [19], Teague and Barrick carried out an electromagnetic modeling study using the Numerical Electromagnetics Code (NEC) to predict the level of Doppler clutter generated by a typical wind turbine.

In this paper, we carry out a more extensive simulation study of the radar scattering from wind turbines in the HF frequency band. We broaden the scope of the work in [19] by studying the clutter behavior in the range-Doppler plane, extending the analysis to scattering from a wind farm instead of a single turbine, investigating potential shadowing created by the farm, and examining some detailed electromagnetic modeling issues. This paper is organized as follows. In Section 2, the modeling methodology and simulation results for a single turbine in the range-Doppler plane are presented first. Next, the analysis is extended to a wind farm modeled as an array of turbines. Section 3 discusses the aliasing of the Doppler spectrum as a result of limited pulse repetition frequency (PRF) of typical HF radars. In Section 4, we study the electromagnetic shadowing caused by wind farms. In Section 5, we discuss some electromagnetic modeling details including the effects of the wire radius, the dielectric material comprising the blades, and the ocean surface. Section 6 is the conclusion.

2. RANGE-DOPPLER FEATURES

Full-wave electromagnetic simulation of a realistic, full size turbine is very time consuming even at HF frequencies, especially if time-varying scattering under blade rotation is to be modeled. To alleviate the computational burden, we model the wind turbine using thin wires, similar to the work of [19]. In Section 5, we shall further discuss the adequacy of using thin wires to model the structure. Full-wave simulations under the thin-wire model are carried out using the method of moment solver in the commercial software FEKO [21]. For our study, the following parameters are used: tower height = 90 m, blade length = 63 m, rotation speed = 15 rpm. The dimensions correspond to the nominal dimensions of a baseline 5-MW offshore wind turbine described in [22]. The entire turbine structure is assumed to be perfectly conducting. An infinite, perfect conducting ground plane

is assumed to model the water surface, which is highly reflecting at HF frequencies. For the HF radar, we assume the antenna is a monopole located at 3000 m from the turbine, and the transmitted wave is incident at edge-on relative to the rotation plane of the turbine blades. The frequency bandwidth is assumed to be 12–14 MHz, leading to a radar range resolution of 75 m. The wire radius in the thin-wire model is assumed to be 0.26 m, which is the maximum allowable under the thin-wire approximation (1/80 of a wavelength at 14 MHz). The range-Doppler image is acquired as follows. First frequency sweep data from 12–14 MHz are collected in steps of 25 kHz. The blades are subsequently rotated 3 degrees and the process is repeated for a complete rotation of the turbine blades. This corresponds to a time sampling rate of 30 Hz at the 15 rpm rotation rate. The simulated data in frequency and aspect are then 2-D Fourier transformed into the range-Doppler plane. A Hanning window is applied to both frequency and aspect dimensions of the data before the Fourier transform.

Figure 1 shows the resulting image in the range-Doppler plane due to a single turbine. The color in the figure is the strength of the scattered signal normalized into dBsm. The strongest feature seen is at the zero Doppler bin, which is due to the stationary tower. The turbine motion has ±9 Hz of Doppler spread for the assumed 15 rpm blade rotation rate at 14 MHz. The periodic nature of the turbine blade return as a function of time causes the Doppler from the rotating blades to be localized in distinct Doppler bins spaced at 3 times the blade rotation rate, or 0.75 Hz. It is observed that even though the

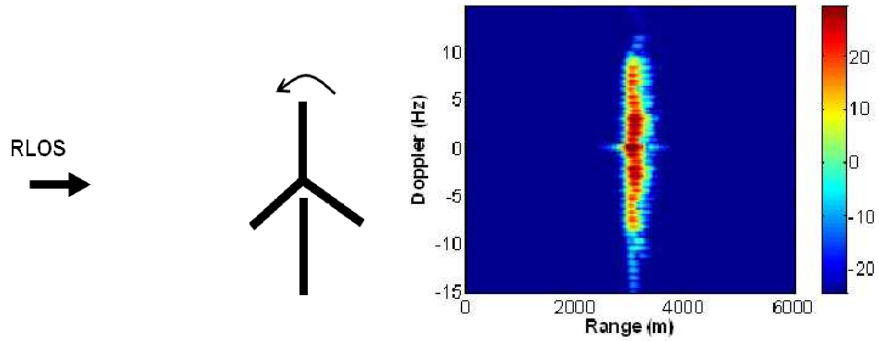

Figure 1. Radar features of a wind turbine rotating above an infinite ground plane. The turbine rotation speed is 15 rpm and the radar frequency range is between 12 and 14 MHz. (a) Simulation set-up using a thin-wire model. (b) Range-Doppler image.

electrical size of the turbine is on the order of the wavelength, range ringing due to resonant scattering is not very prominent.

We next simulate the case of an array of turbines. The spacing between each turbine is assumed to be 1000 m and the source is located 3000 m away from the center turbine. The simulation setup and the resulting range-Doppler image for this case are shown in Figure 2. Figure 2(a) shows the 3×1 turbine array setup. Note that the tower is not shown for clarity in this and the subsequent figures although it is always present in the simulation. In this case, the starting position of a blade of the center turbine is vertically upright while that of the top and bottom turbines is rotated by 20 and 40 degrees respectively. Figure 2(b) is the range-Doppler image for this case. The direct return from the center and the two outer turbines are located respectively in range at 3000 m and 3162 m.

In addition to the direction returns, additional weaker tracks delayed in range are observed that are due to multiple interactions between the turbines. Of the two range-delayed multiple returns seen, the earlier one is due to the interaction between adjacent turbines and is delayed by an extra 581 m as a result. The later return is due to the wave that is re-scattered from a turbine at one edge of the array and is subsequently re-scattered by the turbine on the other edge before returning to the radar resulting in a range delay of 1162 m. Note that these multiple returns are not only weaker, but they show less Doppler content, implying that majority of the multiples take place between the stationary tower structures.

Next, we study the case of a 1×3 turbine array. Figures 3(a) and (b) respectively are the turbine positions and range-Doppler image of

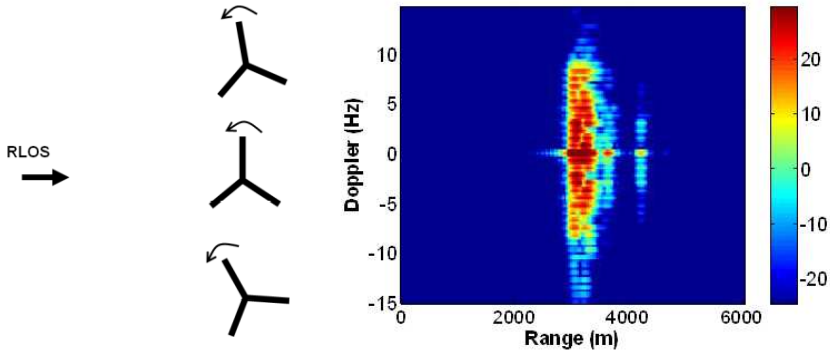

Figure 2. Radar features of a 3×1 wind turbine array. (a) Simulation set-up using thin-wire models. (b) Range-Doppler image.

the 1×3 turbine arrangement. The starting position of the blade of the center turbine is upright while those to its left and right are rotated clockwise by 20 and 40 degrees respectively. In this case, only the direct return from all the turbines is clearly seen. The multiple interactions are expected to be delayed by 1000 m and 2000 m respectively relative to the turbine return in the front.

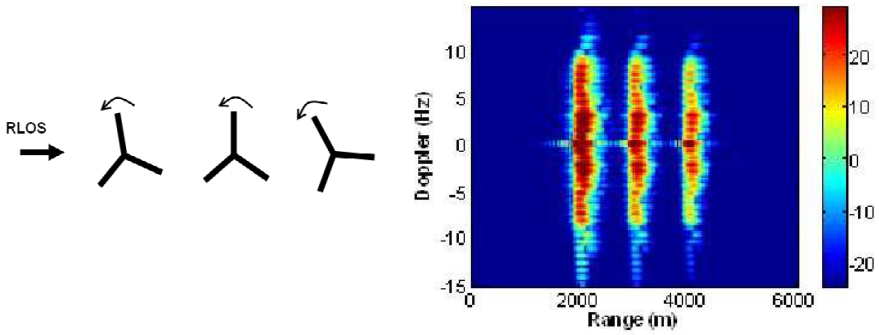

(a) (b)

Figure 3. Radar features of a 1×3 wind turbine array. (a) Simulation set-up using thin-wire models. (b) Range-Doppler image.

Lastly, we simulate the case of a 3×3 turbine array. The starting position of a blade of the turbines in the second row is upright while the blades of the turbines in the first and third row are rotated 20 and 40 degree clockwise with respect to the initial blade position of the turbine in the front row as shown in Figure 2(a). Figure 4(a) shows the setup of the 3×3 array. Figure 4(b) shows the range-Doppler image of the array being excited at edge-on incidence. The features seen can be understood based on the understanding acquired for the case of 1×3 and 3×1 array cases. The return from each column of turbine is clustered together and each cluster is 1000 m apart in range, which corresponds to the physical spacing of the turbine. Additionally, multiple interactions are observed that are due to the wave re-scattering from the tower as discussed for the case of 1×3 turbine array. Figure 4(c) shows the range-Doppler image of the 3×3 case when the position of the monopole excitation is moved such that it makes a 45 degree angle with respect to the horizontal and is located 3000 m away from the center turbine. The maximum radial velocity of the blades relative to the radar decreases, resulting in a decrease in the maximum Doppler spread for the turbines. Six distinct turbines tracks are observed. The 3 missing tracks are due to the returns from turbines overlapping in range.

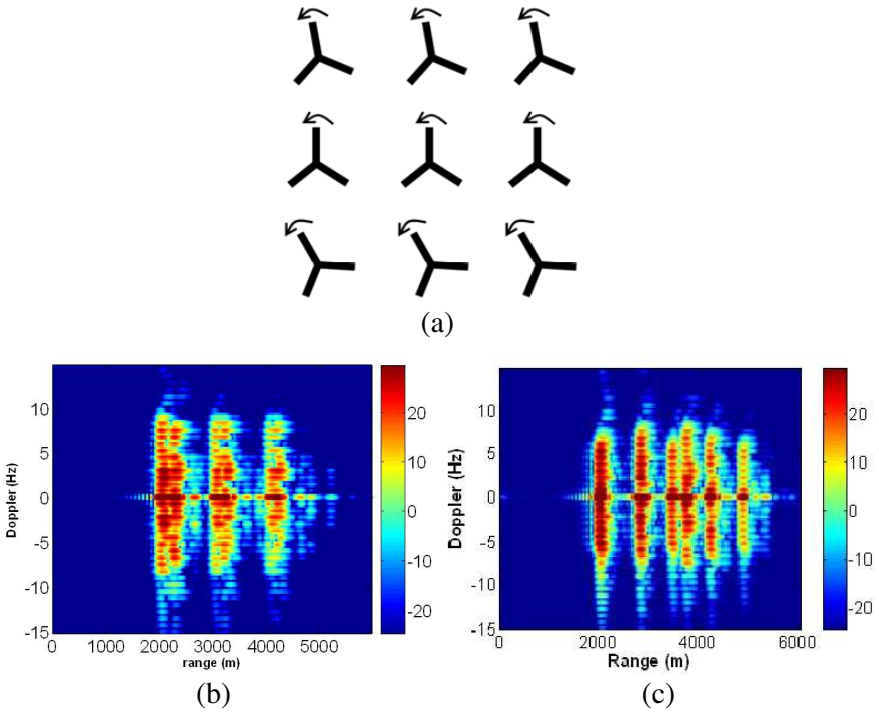

Figure 4. Radar features of a 3×3 wind turbine array. (a) Simulation set-up using thin-wire models. (b) Range-Doppler image under edge-on incidence. (c) Range-Doppler image under 45° oblique incidence.

Overall, we conclude that wind-farm-induced radar scattering is confined in the Doppler dimension to the maximum Doppler of the blades, and in range to the total range extent of the farm. Range-delayed returns due to either intra-turbine or inter-turbine multiple scattering, while present, are fairly weak.

3. DOPPLER ALIASING

The previous section showed non-aliased range-Doppler images of wind turbines. However, the typical PRF of the Coastal Ocean Dyanmics Applications Radar (CODAR) is 2 Hz. As a result, strong aliasing is possible from the turbine signal. This issue was discussed by Teague and Barrick in [19]. The aliasing crowds the Doppler spectrum and can make discerning the turbine features difficult from those of the ocean due to their comparable strengths. Here we simulate the aliasing effect in the Doppler spectrum of a single turbine at a single frequency,

13.5 MHz, in order to get a simple and clear interpretation of the phenomenon.

Figure 5(a) shows the case of the unaliased Doppler spectrum for

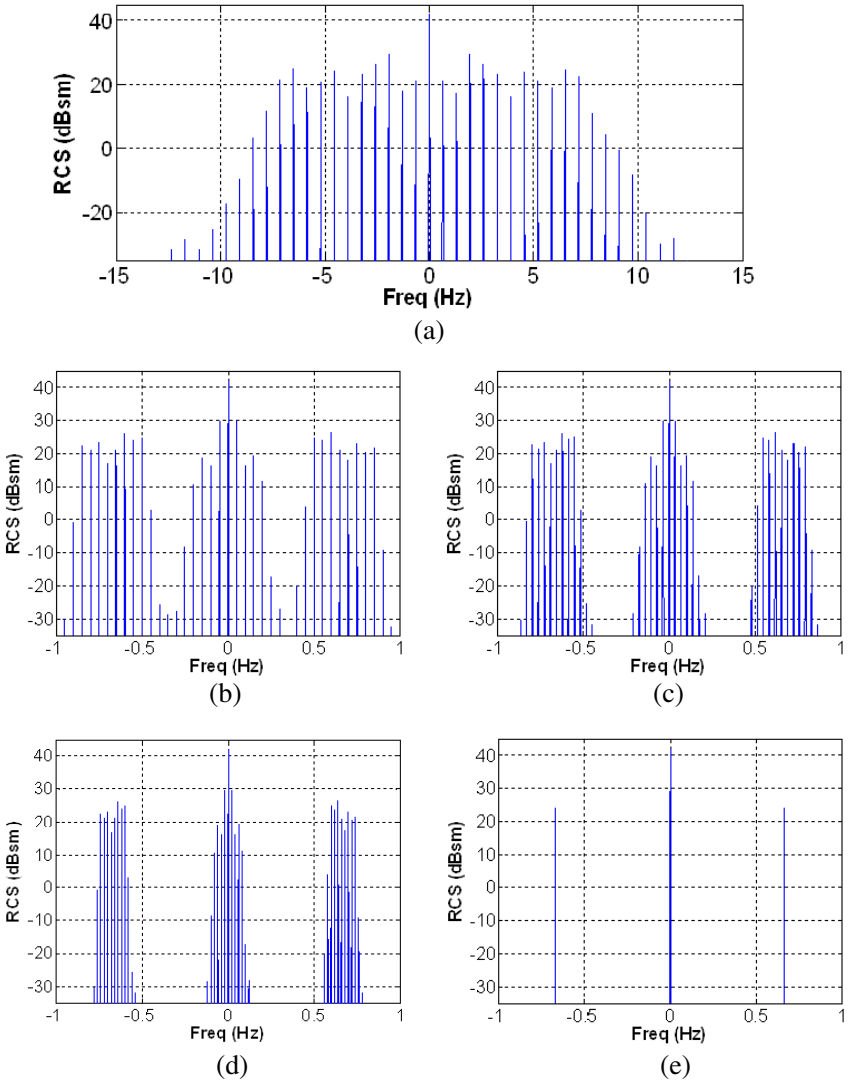

Figure 5. Doppler spectra of a rotating turbine at 13 MHz. (a) 13 rpm rotation speed sampled at 30 Hz. (b) 13 rpm rotation speed sampled at 2 Hz. (c) 13.1 rpm sampled at 2 Hz. (d) 13.2 rpm sampled at 2 Hz. (e) 13.333 rpm sampled at 2 Hz.

a turbine rotating at 13 rpm. The signal is sampled at 30 Hz. The expected Doppler harmonics are located at frequency bins spaced by the rotational frequency of the blades multiplied by three, or 0.65 Hz, since the turbine has 3 blades. Figure 5(b) shows the Doppler spectrum for the same turbine sampled at 2 Hz. As expected, the signal is severely aliased. The first Doppler line is located at the expected value of 0.65 Hz while the next harmonic wraps back to -0.7 Hz in the ± 1 Hz window. With the wrapping process continuing for all the higher harmonics, the spectrum becomes very crowded in the window.

Figures 5(c), (d), and (e) show the Doppler spectra of a turbine rotating at 13.1, 13.2, and 13.333 rpm sampled at 2 Hz. As the rotation rate gets closer to 13.333 rpm, the Doppler lines begin to bunch up. At exactly 13.333 rpm, the Doppler spectrum in Figure 5(e) shows an interesting phenomenon where all the Doppler lines are completely focused into a single frequency bin at 0.667 Hz, which leaves the spectrum very clean. This phenomenon was first observed in [19] and it offers the possibility to focus the Doppler clutter from wind turbines by varying the PRF of the radar. If these lines can be focused at a frequency away from the Bragg peaks due to ocean returns, this scheme could potentially alleviate the interference from wind turbines. Of course, it would require that the turbine rotation rate is fairly steady and that the PRF of the radar can be readily adjusted with high precision to achieve such Doppler focusing.

4. ELECTROMAGNETIC SHADOWING

In addition to examining the radar clutter produced by wind farms, it is also important to study the obstruction (or shadowing) effect produced by wind farms on the potential target (in this case the ocean surface) return. To do so, we simulate the field within and around a wind farm at 13 MHz using FEKO, and compare the results to the field strength in the absence of the farm. Since we expect the tower structure to give the strongest shadowing effect [23], a static blade configuration is assumed in the simulation. Otherwise, the same wind farm parameters are used. The near field plots in two dimensions in the vicinity of a 3×1 turbine array are shown in Figure 6. The horizontal and vertical axes respectively are the range and cross range measured in meters. The fields are calculated at increments of 10 m in both range and cross range. Figure 6(a) shows the field plot (in dB) from a monopole above an infinite conducting plane located on the left at 3000 m away from the plot origin. Figure 6(b) shows the total field plot in the near field of a 1×3 turbine array. Figure 6(c) plots the difference between the field strengths in Figures 6(a) and 6(b). From the figure, it can be seen

that the depth of the electromagnetic shadow, which is the deepest immediately behind each turbine, is less than 2 dB at this frequency.

Additional results are generated for a 3×3 wind farm and shown in Figure 7. Similar to Figure 6, Figure 7(a) shows the field without the farm, 7(b) shows the total field with the farm, and 7(c) shows the difference between the two field strengths. The results are similar to those observed in Figure 6. We do notice a moderate increase in shadow depth for the turbines in the middle row. This means that when a series of turbines are perfectly lined up with respect the radar line-of-sight (RLOS), the shadowing depth gets progressively darker. However, even in this case, the darkest shadow is still within 2 dB of the unperturbed field, and is confined to immediately behind each turbine. Figure 8 shows the situation for the same 3×3 farm when the radar is moved to a 45 degree oblique angle with respect to the center of the farm. Similar findings are observed.

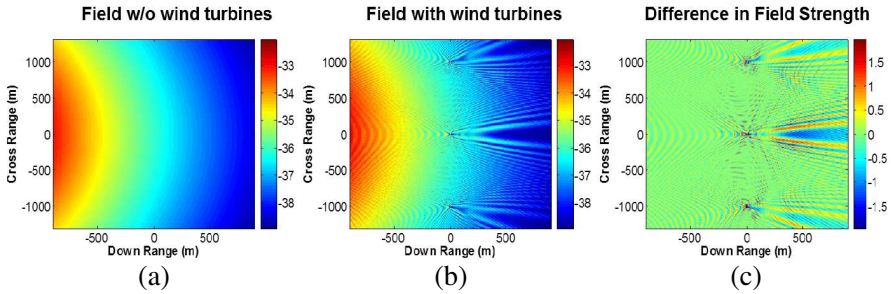

Figure 6. Shadowing effect of wind turbines. (a) Field without wind turbines. (b) Field with a 3×1 wind turbine array. (c) Difference in field strength with and without the turbines.

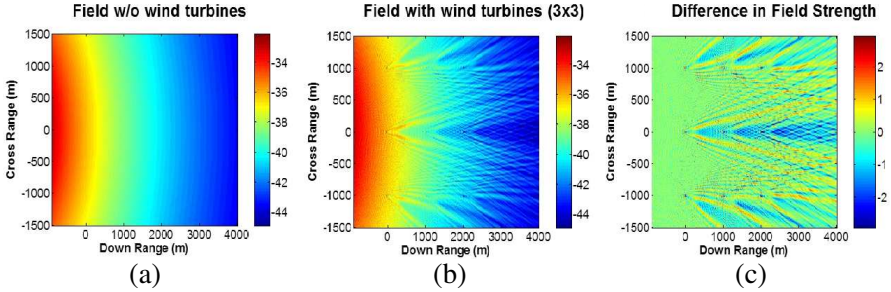

Figure 7. Shadowing effect of wind turbines. (a) Field without wind turbines. (b) Field with a 3×3 wind turbine array. (c) Difference in field strength with and without the turbines.

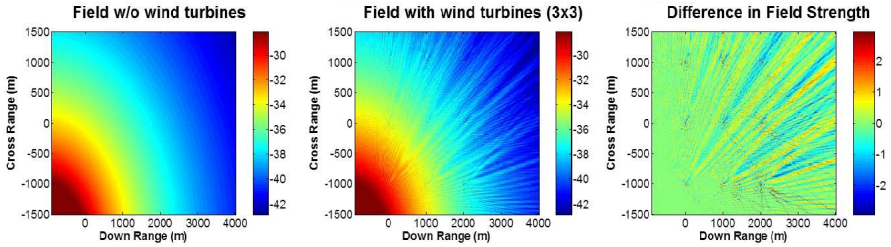

Figure 8. Shadowing effect of wind turbines under 45° oblique incidence. (a) Field without wind turbines. (b) Field with a 3×3 wind turbine array. (c) Difference in field strength with and without the turbines.

5. MODELING DISCUSSION

In this section, the electromagnetic modeling methodology used to generate the simulation results will be discussed in more detail. First the thin-wire approximation is used in this study to save computation time. To address the accuracy of the thin-wire model, we compare the thin-wire result to that from a full surface-mesh model. The components in the surface-mesh model are modeled as circular cylinders with radius of 0.26 m. The length of the components in each model is the same as in the previous sections. Figures 9(a) and 9(b) show the range profiles generated from the thin-wire and surface-mesh models, respectively. A Hanning window is used on the 12–14 MHz data before the inverse Fourier transform. The resulting radar cross section (RCS) is expressed in dBsm. Figures 9(c) and 9(d) show the range-Doppler plots generated from the thin-wire and surface-mesh models, respectively. It can be seen that the results from the two types of modeling are very similar. Of course, the thin-wire model takes much less time to simulate (a factor of approximately 40 for a 3×3 wind farm).

Next, we investigate the effect of wire radius in the thin-wire model. To remain within the validity of the thin-wire approximation, the upper limit on the wire radius is $\square/80$, or 0.27 m at 14 MHz. However, as Figure 10 shows, there does not appear to be a significant change in the RCS level as the cylinder radius is extended from 0.27 m to 1 m for the full-surface mesh model. In this case, only the 90 m cylindrical tower structure is analyzed for simplicity. On the other hand, when the thin-wire radius is reduced from 0.27 m down to 0.027 m then to 0.0027 m, there begins to be stronger resonant ringing

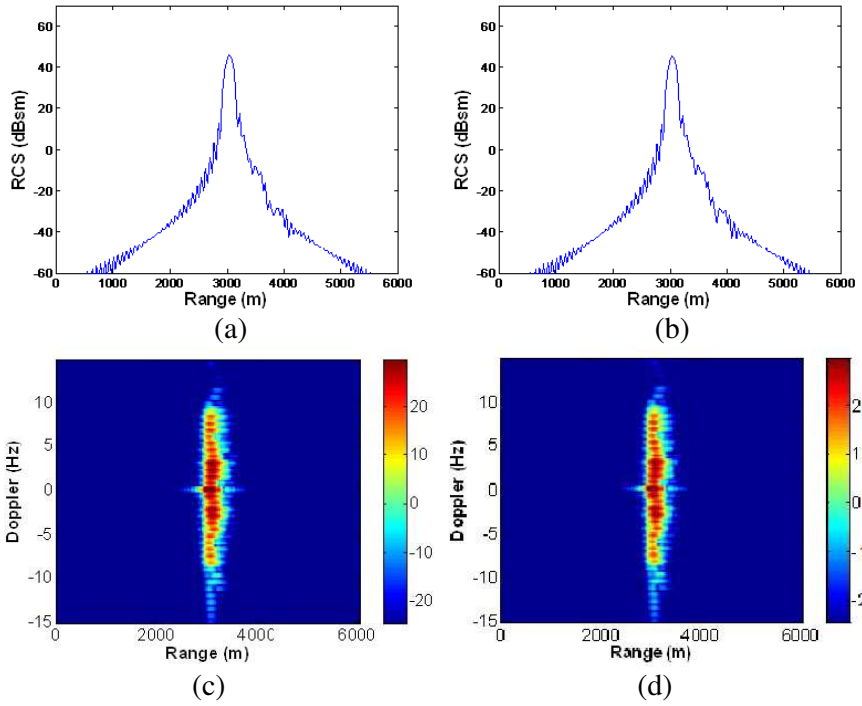

Figure 9. Comparison between the full surface-mesh model and the approximate thin-wire model computed using FEKO. The blades and tower of the model have a radius of 0.26 m. (a) Range profile from the surface-mesh model. (b) Range profile from the thin-wire model. (c) Range-Doppler plot from the surface-mesh model. (d) Range-Doppler plot from the thin-wire model.

in range, as shown in Figures 11(a) to 11(c). This is caused by the strongly guided traveling wave along a very thin wire, which makes multiple traversals along the wire. This traveling wave is not expected to be strongly supported in a real turbine structure due to both its larger radius and non-uniform cross section. Therefore, it is a good practice to keep the wire radius at close to its upper limit ($\square/80$) for the thin-wire modeling of wind turbines.

Next, we investigate the effects of non-perfect-conducting material of the turbine components on the scattered signal from the turbine, since perfect conducting wires were used to generate the results in the previous sections. Figure 12 presents a comparison between a dielectric and a perfect electric conducting (PEC) cylinder of height 90 m and radius 1 m computed using the surface mesh model. The

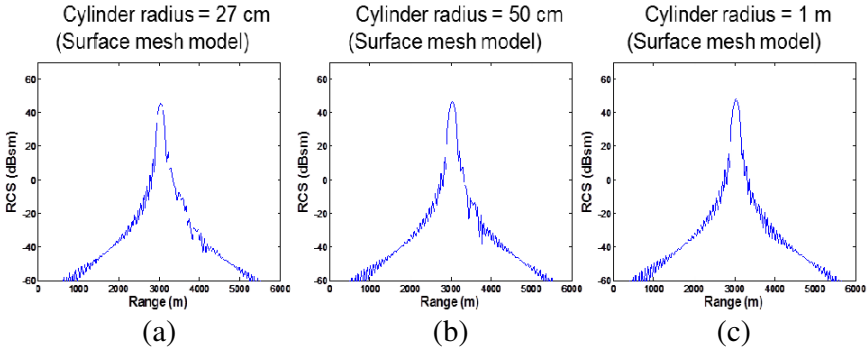

Figure 10. Effect of increasing the cylinder radius in the surface-mesh model on the range profile of a 90 m tower. The frequency range is from 12 to 14 MHz.

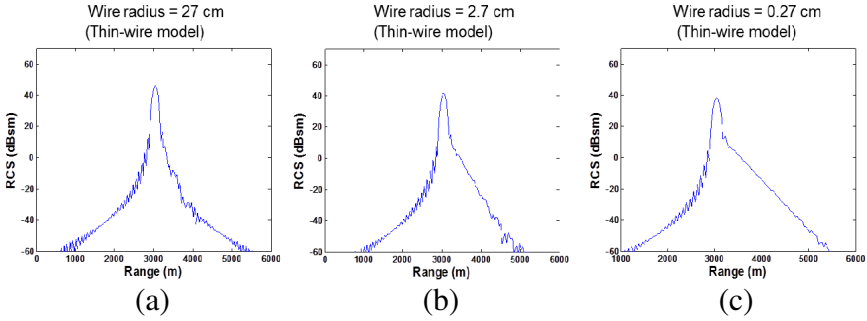

Figure 11. Effect of decreasing the wire radius in the thin-wire model on the range profile of a 90 m tower. The frequency range is from 12 to 14 MHz.

full-wave surface integral equation solver is used in FEKO for the dielectric cylinder. The material is assumed to be carbon fiber and the real part of the relative permittivity is taken to be 20 while the imaginary part is 0.15 [24]. Figures 12(a) and (b) show the frequency responses for respectively the dielectric and PEC cases from 10 to 20 MHz. It is observed that the dielectric scattering is higher by about 3 dB. The conducting cylinder shows slight undulations over the whole range. Figures 12(c) and (d) are the corresponding range profiles of the 12–14 MHz data of the two cases. It is observed that the range characteristics are largely similar, except the range peak due to the dielectric material is about 3 dB higher than the case of the PEC cylinder.

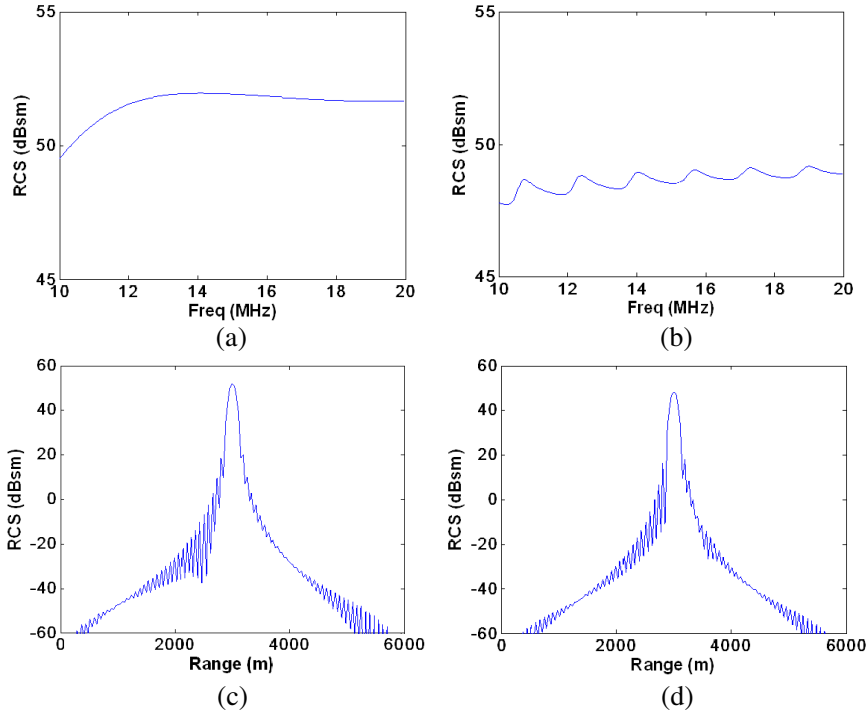

Figure 12. Effect of turbine material on the RCS. (a) Dielectric cylinder frequency response. (b) PEC cylinder frequency response. (c) Dielectric cylinder range profile. (d) PEC cylinder range profile.

Finally, we examine the effect of the ground plane, which is used to model the sea surface, on the observed RCS level. A detailed study on the ground plane effect to wind turbine RCS at microwave frequency range was reported in [25]. Here, we extend the analysis to the HF frequency range. For the configuration at hand where the transmitter is a monopole located on the surface of the ground plane, the scattered field strength is approximately increased by a factor of four from that of the free-standing structure. This comes from the additional single and double ground bounced returns as shown in Figure 13(a). Due to the vertical polarization and the on-surface nature of both the transmitter and the scatterer, these four contributions add coherently in phase. This factor-of-four amplification in field leads to a factor of 16, or 12 dB, increase in RCS. Of course, this argument ignores the interaction between the scatterer and its image. Figures 13(b)–(c) illustrates this point. The simulation is conducted both with the ground (Figure 13(b)) and without the ground (Figure 13(c)) and the

range profiles are plotted for different blade rotation angles. The difference in dB scale between the result in Figure 13(b) and four times that of Figure 13(c) is shown in Figure 13(d). We can see that the difference is not large, demonstrating that the approximate 12 dB argument is obeyed. Nonetheless, the difference is not zero, as there exist non-negligible higher-order interactions between the turbine and the ground plane.

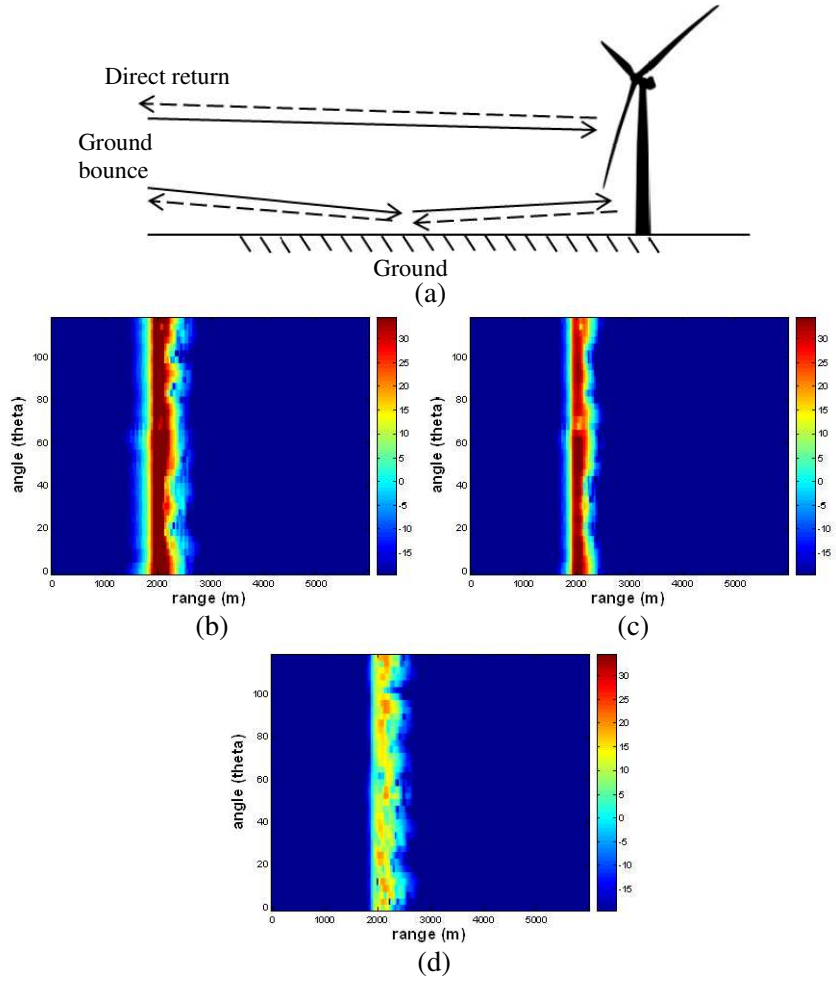

Figure 13. Effect of the conducting ground surface on the turbine RCS. (a) Possible ground bounce mechanisms. (b) RCS versus range and blade angle in the presence of ground. (c) RCS versus range and blade angle without ground. (d) Difference between the with-ground case and four times the without ground case.

6. CONCLUSION

The radar features of a single and arrays of wind turbines have been simulated and studied in the HF frequency band. The scope of the investigation in [19] has been extended by studying the clutter behavior in the range-Doppler plane, broadening the analysis to scattering from a wind farm instead of a single turbine, investigating potential shadowing created by the farm, and examining some detailed electromagnetic modeling issues. It was found that wind-farm-induced radar scattering is confined in the Doppler dimension to the maximum Doppler from the blades, and in range to the total range extent of the farm. Range-delayed returns due to either intra-turbine or inter-turbine multiple scattering, while present, are fairly weak. It was also found that when the radar PRF is low compared to the maximum Doppler from the blades, strong aliasing occurs that results in a crowded Doppler spectrum. If the PRF of the radar can be precisely controlled relative to the blade rotation rate, it may be possible to focus the Doppler lines into a few Doppler frequency bins. In addition, the overall shadowing effect of a wind farm was found to be not very prominent in the HF regime. The shadow depth is at most 2 dB in the immediate vicinity behind each turbine away from the radar. There is a moderate increase in shadow depth behind a turbine that is in the shadow of another turbine. Finally, electromagnetic modeling details including the effects of thin-wire modeling, non-conducting turbine components, and the presence of a conducting ground surface were examined. With the growing development of wind farms in the world's coastal oceans, their effects on HF radar ocean applications warrant further studies, especially in conjunction with other factors influencing the performance of HF radar in ocean current and wave mapping [20].

ACKNOWLEDGMENT

This work was supported by the National Science Foundation under Grant ECCS-1232152, and in part by the Department of Energy under Grant DE-EE0005380.

REFERENCES

1. Special Evaluation Report to Assess Effect of Wind Turbine Farm on Air Route Surveillance Radar-4 at King Mountain, Texas, USAF 84 RADES & FAA, May 30, 2002.
2. The Effects of Wind Turbine Farms on ATC RADARS, Air Warfare Center, Royal Air Force, UK, May 10, 2005.

3. Further Evidence of the Effects of Wind Turbine Farms on AD RADARS, Air Warfare Center, Royal Air Force, UK, Aug. 12, 2005.
4. Report to the Congressional Defense Committees on The Effect of Windmill Farms on Military Readiness, Office of the Director of Defense Research and Engineering, Undersecretary for Space and Sensor Systems, Aug. 2006.
5. Lemmon, J. J., J. E. Carroll, F. H. Sanders, and D. Turner, "Assessment of the effects of wind turbines on air traffic control radars," NTIA Technical Report TR-08-454 to the U.S. Department of Commerce, Jul. 2008.
6. Brenner, M., "Wind farm and radar," The MITRE Corp., Report JSR-08-125 to the Dept. of Homeland Security, Jan. 2008.
7. Impact of Wind Turbines on Weather Radars, OPERA II WP 1.8, 2006.
8. Sandifer, J. B., T. Crum, E. Ciardi, and R. Guenther, "A way forward: Wind farm-weather radar coexistence," *WINDPOWER 2009*, Chicago, IL, May 2009.
9. Hood, K., S. Torres, and R. Palmer, "Automatic detection of wind turbine clutter for weather radars," *J. Atmosph. Ocean. Tech.*, Vol. 27, 1868–1880, May 2010.
10. Belmonte, A. and X. Fabregas, "Analysis of wind turbines blockage on doppler weather radar beams," *IEEE Antennas Wireless Propagat. Lett.*, Vol. 9, 670–673, 2010.
11. Ling, H., M. F. Hamilton, R. Bhalla, W. E. Brown, T. A. Hay, N. J. Whitelonis, S.-T. Yang and A. Naqvi, "Assessment of offshore wind farm effects on sea surface, subsurface and airborne electronic system," Final Report for DE-EE0005380, Dept. of Energy, Sept. 2013.
12. Poupart, G. J., "Wind farms impact on radar aviation interests," QinetiQ Corp., Final Report to the Dept. of Trade and Industry, UK, Sept. 2003.
13. Hill, K. C., G. Zelinski, T. Van, and C. Vogel, "Computational electromagnetics (CEM) prediction of a windmill," *2007 Electromagnetics Code Consortium Annual Meeting*, May 2007.
14. Kent, B. M., A. Buterbaugh, K. C. Hill, G. Zelinski, R. Hawley, L. Cravens, T. Van, C. Vogel, and T. Coveyou, "Dynamic radar cross section and radar doppler measurements of commercial general electric windmill power turbines Part 1 — Predicted and measured radar signatures," *IEEE Antennas Propag. Magazine*, Vol. 50, No. 2, 211–219, Apr. 2008.

15. Kent, B. M., A. Buterbaugh, K. C. Hill, G. Zelinski, R. Hawley, L. Cravens, T. Van, C. Vogel, and T. Coveyou, "Dynamic radar cross section and radar doppler measurements of commercial general electric windmill power turbines Part 2 — Predicted and measured radar signatures," *Proc. 2007 AMTA Symposium*, St. Louis, MO, 2007.
16. Naqvi, A., S.-T. Yang, and H. Ling, "Investigation of doppler features from wind turbine scattering," *IEEE Antennas Wireless Propagat. Lett.*, Vol. 9, 485–488, 2010.
17. Greving, G., W. Biermann, and R. Mundt, "Wind turbines as distorting scattering objects for radar — Clutter aspects and visibility," *Proc. Int. Radar Symp.*, Vilnius, Lithuania, Jun. 2010.
18. Wyatt, L. R., A. M. Robinson, and M. J. Howarth, "Wind farm impacts on HF radar current and wave measurements in Liverpool Bay," *Proc. IEEE OCEANS Conference*, Santander, Spain, Jun. 2011.
19. Teague, C. C. and D. E. Barrick, "Estimation of wind turbine radar signature at 13.5 MHz," *Proc. IEEE OCEANS Conference*, Hampton Roads, VA, Oct. 2012.
20. Liu, Y., R. H. Weisberg, C. R. Merz, S. Lichtenwalner, and G. J. Kirkpatrick, "HF radar performance in a low-energy environment: CODAR SeaSonde experience on the west florida shelf," *J. Atmosph. Ocean. Tech.*, Vol. 27, 1689–1710, Oct. 2010.
21. FEKO version 6.2, EM Software & Systems Inc., Stellenbosch, South Africa, 2012.
22. Jonkman, J., S. Butterfield, W. Musial, and G. Scott, "Definition of a 5-MW reference wind turbine for offshore system development," National Renewable Energy Laboratory, Tech. Rept. NREL/TP-500-38060, Feb. 2009.
23. Yang, S.-T. and H. Ling, "Electromagnetic simulation of the near-field distribution around a wind farm," *Int. J. Antennas Propagat.*, Vol. 2013, Article ID 105071, 9 Pages, 2013.
24. Dang, Z., J. Wu, H. Xu, S. Yao, and M. Jiang, "Dielectric properties of upright carbon fiber filled poly (vinylidene fluoride) composite with low percolation threshold and weak temperature dependence," *App. Phys. Lett.*, Vol. 91, 072912, 1–3, 2007.
25. Naqvi, A., N. Whitelonis, and H. Ling, "Doppler features from wind turbine scattering in the presence of ground," *Progress In Electromagnetics Research Letters*, Vol. 35, 1–10, 2012.